Fast plasma production by intense femtosecond extreme ultraviolet and x-ray pulses

C. Fasolato,[1,*] E. Stellino,[2,†] F. Sacchetti,[3,4] and C. Petrillo[3,5]
[1]*CNR-ISC, Istituto dei Sistemi Complessi, I-00185 Roma, Italy*
[2]*Sapienza Università di Roma, Dipartimento di Scienze di Base e Applicate per l'Ingegneria, I-00185 Roma, Italy*
[3]*Università di Perugia, Dipartimento di Fisica e Geologia, I-06123 Perugia, Italy*
[4]*CNR-IOM, Istituto Officina dei Materiali, I-06123 Perugia, Italy*
[5]*AREA Science Park, I-34149 Padriciano, Trieste, Italy*

(Received 5 July 2024; accepted 28 November 2024; published 21 January 2025)

We develop a semiempirical model to describe the creation of an electron plasma in matter at extreme conditions, as excited by high-intensity, extreme ultraviolet (EUV) or x-ray radiation pulses currently available at free-electron laser (FEL) facilities. In typical FEL experiments, EUV and x-ray pulses are used to investigate highly excited states of matter produced by optical pump pulses. The pump pulses, promoting electrons from delocalized valence band states, excite the system often through multiphoton absorption processes and/or shock wave propagation. Instead, the use of FEL radiation as a pump allows triggering electron transitions from bound, core states to nearly free levels above the Fermi energy, promptly generating a highly excited state, toward the warm dense matter regime. We model such an excitation process starting from the optical properties of the analyzed materials and first-principle considerations, with the aim of motivating further studies in this scheme. We apply our model to predict the differences in the plasma creation process in insulators and metals, at varying exciting pulse wavelength and fluence, and we interpret the results in terms of the different nature of the investigated systems. Furthermore, we explore the effect of the finite core hole lifetime on the plasma formation and relaxation dynamics. We show the model is suited for the interpretation of real experimental data obtained from a prototypical insulating crystal (LiF) in a EUV FEL pump–optical transmission probe experiment.

DOI: 10.1103/PhysRevResearch.7.013072

I. INTRODUCTION

The recent development of free electron laser (FEL) sources has enabled a large variety of new experiments, opening the possibility of studying radiation-matter interaction directly in the time domain, in the pump-probe scheme, achieving femtosecond resolution in a hardly explored wavelength region, from the extreme ultraviolet (EUV) to x-rays, i.e., up to several tens of keV [1–6]. In typical experiments, a pump pulse with sharp time resolution modifies the state of the sample, while a properly synchronized FEL probe pulse is employed to measure the time evolution of the system absorption, reflection, or scattering. Two important points must be carefully considered to perform experiments providing meaningful data, for a correct interpretation of the sample behavior. The first aspect is the need for an adequate probe, intense enough to produce a measurable signal in a short time, while weak enough to allow interpreting the data within the linear response approximation or, in any case, to produce a minimum additional state change. The nonlinearity of the probe response can be due to both its intensity and its coherence [6], which is implicit in this sort of experiment, where both pump and probe are produced by laser or laser-like processes. The second point is the need for a pump that affects the sample state uniformly, in a scattering volume larger than the region sampled by the probe.

When an optical (infrared/visible/ultraviolet, IR/Vis/UV) laser is used as a pump, the control of the pumped volume is hardly achieved: the release of energy is complex and its propagation can be slow in the experimental timescale. Nevertheless, several experiments have been performed in this way, and there exists some protocol to obtain good data [7]. An additional problem linked to the use of an optical pump is the fact that the plasma produced by photoexcitation has a significant reflectivity in this wavelength range, so that part of the pump energy can be reflected, making the excitation process even more complex and, possibly, poorly efficient [8]. In an alternative scheme, FEL radiation can act as a pump, while FEL pulses of a different wavelength (in the so-called two-colors approach) [9] or optical lasers [10], depending on the nature of the experiment, are exploited as probes. Interestingly, compared to the former scheme, FEL pumping triggers a process with a different time evolution: in a short time during the absorption [11], the FEL pump photoexcitation is expected to produce a plasma of rather high atomic and energy density, enabling the study of this exotic state of matter.

*Contact author: claudia.fasolato@cnr.it
†Contact author: elena.stellino@uniroma1.it

Published by the American Physical Society under the terms of the Creative Commons Attribution 4.0 International license. Further distribution of this work must maintain attribution to the author(s) and the published article's title, journal citation, and DOI.

In this paper, we introduce a semiempirical model for the fast sample excitation produced by an intense radiation pulse in the EUV range or beyond, up to the soft x-ray region. The model is useful to describe the short-time evolution of the sample state. We focus on material systems, like LiF, diamond, MgO, and MgF_2, that are transparent in the IR/Vis/UV range, in which EUV pumping can produce the fast excitation of an absorbing plasma, so that the sample acquires in the probe region a significant absorbance, depending on the electron density. We then compare the results with those expected for simple metals. The present model is not to be considered as a comprehensive, predictive theory, but rather as a guide for the design and interpretation of experiments employing extreme ultraviolet soft x-ray radiation pulses in the discussed scheme. For a more complete theory, although in a different exciting energy density condition, we refer the reader to other recent works [12].

The interaction of materials with short wavelength radiation is significantly different from that with optical radiation. Optical (IR/Vis/UV) pumping excites electrons from delocalized valence states and produces the formation of hole states close to the Fermi level, with subpicosecond lifetimes. Indeed, hole annihilation can occur (1) by electron-radiation interaction, involving two electron states and one photon state (radiative decay, slower process), and (2) through Coulomb electron-electron interaction, involving four electron states and no photon state (Auger nonradiative decay, faster process). On the other hand, no matter whether the sample is metallic or insulating, a high-photon-energy (x-ray to EUV) pump triggers the transition of electrons from bound, localized states to almost-free states above the Fermi level, transforming the sample locally into an excited plasma, with no possibility of returning to the original condition. Due to the short lifetime of almost-free electron states, a sort of thermodynamic equilibrium of the electron subsystem is obtained rather promptly. Such delocalization of excited electron states produces a much longer lifetime of the core holes, with the nuclear motion entering the process in the picosecond time scale [10].

In our model, at a first stage it is assumed that the core hole annihilation is negligible at the timescale of the excitation process. The plasma properties are examined as a function of the exciting energy density and wavelength, depending on the material optical functions. In a refined version of the model, the density and lifetime of the core holes is considered. The results of the present simulations are compared to an experimental test on a crystalline sample of LiF carried out at the TIMEX beamline [13] (FERMI FEL, Trieste, Italy [3]). Additional estimates are produced in the case of typical metals K and Fe, where the initial metallic state produces a high reflectivity in the Vis region and a rather high absorption in the soft x-ray range. In this case, the properties of the plasma created by pump absorption are different as compared to the insulator case.

II. EMPIRICAL MODEL

We here propose an empirical model to describe the absorption process of a short EUV to soft x-ray pulse, and the consequent fast creation of a plasma of excited electrons in almost-free states in a relatively wide, confined, and uniformly excited sample volume. The absorption of high-energy photons produces an abrupt decrease in the absorption cross section of the sample by reducing the occupation of the core electron states, thus allowing for the propagation of the exciting pulse within the sample. Much differently, a low-energy IR/Vis/UV pump is typically absorbed in a shorter path, the excited electrons producing a plasma with high-enough density to continue the optical absorption process in the same sample region. In other words, the high-energy excitation produces, in a short time, a larger volume where excited electron states are present at lower density as compared to optical pumping.

Firstly, the model is applied to specific examples in which the sample is transparent to the IR/Vis/UV radiation while having a low-enough EUV transmission to produce an electron plasma with appropriate density. As a second case study, we then consider metals like K and Fe, in which the initial conditions are basically the opposite, due to differences in both the atomic density and the wavelength dependence of the absorption coefficient.

We start by defining the absorption coefficient $\mu(\lambda)$ and the reflectivity $R(\lambda)$ of the original sample in terms of the complex refractive index $\tilde{n}(\lambda) = n(\lambda) + ik(\lambda)$, $n(\lambda)$ and $k(\lambda)$ being the usual optical constants:

$$\mu(\lambda) = \frac{4\pi k(\lambda)}{\lambda} \tag{1}$$

and

$$R(\lambda) = \frac{[1 - n(\lambda)]^2 + k(\lambda)^2}{[1 + n(\lambda)]^2 + k(\lambda)^2}. \tag{2}$$

Both $n(\lambda)$ and $k(\lambda)$ are available with good accuracy in a wide wavelength range [14] for many solid and liquid samples: therefore, the ground-state optical properties can be considered as known. In the case of a time-dependent excitation of the sample, $n(\lambda)$ and $k(\lambda)$ start displaying a time dependence too. However, considering that if $\lambda < 0.1\,\mu$m, the wave period is less than 0.3 fs, i.e., 100 times smaller than a pulse duration of 30 fs, one can safely consider the optical constants as slowly varying, stationary properties.

The effect of the fast radiation absorption, and consequent electron excitation, was clearly observed in transmission experiments using both EUV [15–17] and keV x-ray at very high energy density [18]. An evident nonlinear increase of the transmission of a thin slab, as a function of the pulse energy, was observed in different materials. Of course, these studies measure the transmission of the short-wavelength beam with no time resolution, as they are probe-only experiments typically using conventional detectors.

To quantitatively describe the EUV absorption process, one needs to consider the decrease of the absorption coefficient $\mu(\lambda)$, which depends on the number of electron transitions from the ground state to the excited state. This, in turn, is equal to the number of photons absorbed from the incoming beam in a given space volume $d\Omega = Sdx$ in the time interval dt, S being the beam cross section through the sample and dx the arbitrarily small thickness. The reflectivity of the system after the excitation can also contribute to the apparent transmission. In thick metallic samples, the transmission cannot be

measured, but a pump-probe measurement of the reflectivity in the IR/Vis/UV range would be possible, providing access to some information on the state of the plasma produced by EUV/soft-x-ray excitation.

To perform a simulation of the sample excitation, we consider that the number of electron transitions is equal to the difference between the corresponding average occupation number per atom in the ground state in the unperturbed system Z_0 and in the excited system. We define the latter as the time- and space-dependent core-state occupation number $Z(x,t)$, at distance x from the sample surface and at time t from the reference arrival time at $x = 0$. The number of transitions dN_t, per unit time, at a given space-time point (x,t), is given in the following differential form:

$$dN_t = -dI_b = \mu(x,t)\, I_b(x, t - t_p)\, dx = \mu(x,t) N_0 f(x,t)\, dx, \tag{3}$$

where $I_b(x,t) = N_0 f(x,t)$ is the incoming photon flux, with $f(x,t)$ the properly normalized pump photon density and N_0 the number of incident photons; $\mu(x,t)$ is the linear absorption coefficient as a function of space and time, including the (small, as compared to pulse duration) radiation propagation time $t_p = t - x/c$, where we have acknowledged the quasi-transparent nature of the created plasma [10]. The function $f(x,t)$ satisfies a boundary condition $f(0,t) = f_0(t)$, $f_0(t)$ describing the time dependence of the EUV pulse, with $\int_{-\infty}^{+\infty} f_0(t)dt = 1$.

The linear absorption coefficient accounts for two contributions, namely, that from the absorption depending on the population of the core states, and that due to the excited electron plasma $\mu_{\rm pl}(x,t)$, expected to be negligible when the photon energy increases. Considering that the core holes are localized, we can assume a local modification of the system optical properties by photoexcitation. We stress that, in this way, we implement a nonlinearity in the model by introducing a radiation-induced modification of the system properties. We do not consider any nonlinearity in radiation-matter interaction, consistently with quantum electrodynamics [6]. The variation of the absorption coefficient at (x,t), in the time interval dt, is thus described to be proportional to the (negative, as discussed below) variation of the average core state occupation number $Z(x,t)$.

We can use the following:

$$d\mu = \frac{\nu}{Z_0}\, \mu_0\, dZ,$$

where μ_0 is the absorption of the unperturbed atom and ν is the number of nearby atoms, whose absorption cross section is expected to be strongly affected by the absorption event. Indeed, the absorption causes the transition of an electron to a delocalized state, strongly decreasing the probability of a second transition from the core states of the nearest neighbors, in a similar fashion as a second ionization in a molecule. Taking as ν the number of first nearest neighbors might be a good starting point for an evaluation, considering that an accurate experiment can help to fully understand this aspect of the process.

One must note that, locally, there is not a continuous variation of the absorption cross section because the local occupation number is an integer. However, for the simulation of the process, we only need the average occupation number $Z(x,t)$. The variation dZ of the average core-state occupation number is proportional to the absorption of the incoming beam in the time interval dt:

$$dZ = -\alpha\, f(x,t) dt.$$

Finally, we have

$$d\mu = -\frac{\nu}{Z_0}\, \mu_0\, \alpha f(x,t) dt \tag{4}$$

Accordingly, to get a formal estimate of the proportionality constant α we observe that, given the atomic density $n_{\rm at}$, in the (small) sample volume $d\Omega = S dx$, there are $dN_{\rm at} = n_{\rm at} S dx$ atoms, but only a fraction proportional to $Z(x,t)/Z_0$ has the full absorption cross section because, as discussed above, once an electronic transition has occurred, a second transition from the same site (or from the neighboring atoms) is very unlikely. Here, $n_{\rm at}$ refers to one atom of the formula unit, because at a given wavelength one core state is primarily contributing to the absorption. Therefore, one has

$$\alpha = \frac{N_0 \mu_0}{n_{\rm at} S} \tag{5}$$

In principle, one could calculate $\mu(x,t)$ using a theoretical approach like time-dependent density functional theory [19,20], at least when the radiation wavelength is not too short so that the basic approximation of this technique is fulfilled [19]. However, detailed calculations are difficult and there is the need for some additional approximation, so that the results are useful for a comparison to an experiment, while one is more interested in a model able to obtain specific quantitative information from the data and, possibly, to provide a guideline for new investigations.

The above equations (3) and (4) can be solved numerically at a good accuracy level once the basic quantities μ_0 and $n_{\rm at}$ are known, and the total energy $E_{\rm tot}$ and wavelength of the incoming radiation are defined. The solution of the equations allows for the determination of the *average* number of excited electrons $Z_0 - Z(x,t)$ and the corresponding density of the plasma defined as

$$n_{\rm pl}(x,t) = \frac{[Z_0 - Z(x,t)]}{\Omega_a} = \frac{Z_{\rm pl}(x,t)}{\Omega_a} = \frac{3}{4\pi\,[a_0\, r_s(x,t)]^3}, \tag{6}$$

where Ω_a is the atomic volume and the last equality is written in terms of the plasma density parameter $r_s(x,t)$ dependent on position and time, and a_0 is the Bohr radius.

According to the fact that in a very short time [11] an excited plasma is produced by the pump, it is possible to investigate some properties of the new state of the sample using the characteristics of the plasma resonance expected in that condition. A simple description of the plasma resonance can be based on the basic approach proposed in Ref. [21], useful for a straightforward comparison to the experimental data. Experiments provide the plasma transmission spectrum, and hence the product $\mu_{\rm pl}(\lambda)d$ of the plasma, having absorption coefficient $\mu_{\rm pl}(\lambda)$ and thickness d. This comparison is complicated by the fact that the electron density of the plasma is not constant, as a consequence of both the complexity of the plasma creation process and the intrinsic spatial variation of

the energy of the incoming radiation pulse. The macroscopic measurement of the sample transmission provides only a spatial average of $\mu_{\rm pl}(\lambda)d$. Therefore, it is necessary to employ a proper model of the sample response. In this sort of standard pump and probe experiment, a time resolution better than 0.1 ps is well within the technical capability [22]. A specific example will be discussed in the next sections by analyzing the data available from an experiment performed on LiF [10]. To appreciate the effect of the spatial inhomogeneity suggested by the present study, however, a time resolution overcoming the pulse duration would be necessary.

III. APPLICATION OF THE MODEL TO BENCHMARK SAMPLES

To define the characteristics of the proposed plasma creation model, we first consider typical materials that are transparent to the visible light, while markedly absorbing the EUV radiation. These samples can be interesting and informative, because the plasma created by the EUV excitation makes the sample absorbing in the visible range. The transparent systems are diamond (C), magnesium difluoride (MgF_2), and magnesium oxide (MgO), all systems for which the optical constants are available in a wide wavelength interval. Eventually, we describe the case of LiF, in which experimental information on EUV absorption and its effect in the visible region, from a pump and probe experiment, is available [10] and optical constants are known. As a different case study, we consider visible-light-absorbing materials. Specifically, we selected the metals potassium (K) and iron (Fe), the first being a simple metal with low atomic and electronic density, while the second is a transition metal with high atomic density and complex, strongly interacting electron states.

For each sample we simulate the trend of the radiation intensity as a function of time and penetration depth and the time evolution of the plasma density, by a numerical integration of the coupled differential Eqs. (3) and (4). Considering the fact that, as discussed above, a single absorption of a high-energy photon already changes strongly the local atomic state, we used $Z_0 = 1$ everywhere to attempt an overview of the effect of EUV excitation. The conditions used in the different systems are given in Table I, where we report the incoming photon wavelength λ, $\mu_0(\lambda)$ and the atomic number density $n_{\rm at}$. All the tests are performed using an incoming beam having a total energy of 15 μJ per pulse, a duration of 80 fs, and focused on the sample in a circular spot of 30 μm in diameter, thus obtaining an average power density of $\sim$27 TW/cm^2. The power and duration were those used in the LiF experiment [10], useful for a comparison with actual experimental results. Of course, since the tests are performed using different incoming wavelengths, and hence different photon energies, the equivalent number of photon per pulse changes depending on the wavelength.

In Figs. 1(a) and 1(c), we report typical EUV intensities through the sample, as a function of position and time, in the case of MgO and MgF_2 at two wavelengths. The color map is such that a vertical cut in the graph describes the temporal evolution of the EUV intensity experienced in a point at a depth x from the sample surface. A horizontal cut gives the instantaneous spatial distribution of the pulse intensity at a time t.

A typical behavior is obtained when the absorption coefficient as well as the parameter α are high enough. Under this condition, the fast reduction of the absorption coefficient as described in Eq. (4) allows for a tiny intensity reduction, at the expense of the time length of the incoming radiation pulse. As a consequence, the radiation penetrates the sample up to a distance d (see Table I) where the pulse duration approaches zero, while the peak intensity remains almost constant. This behavior is similar in the insulating samples, with variations due to a combination of the linear absorption coefficient and the atomic density of the sample. We recall that this is just an asymptotic behavior obtained as a mathematical solution for our problem, since the model is developed under the limit of pulse duration greater than the radiation period ($\sim$0.1 fs for 40 nm wavelength).

In Figs. 1(e) and 1(g), we show the results for the two metals potassium and iron. Interestingly, the two samples show a common behavior, somewhat different from that of the transparent samples. In the case of shortest wavelength (20 nm), the absorption coefficient is small enough and the intensity decreases exponentially, as is usual when a weak beam of radiation impinges upon a sample. Additionally, there is no simple relation between the duration of the pulse and the depth into the sample, as is the case of transparent samples.

As the wavelength becomes longer, the absorption coefficient increases and, at the same time, also α increases. Therefore, in the limit of large wavelengths, the behavior observed in the transparent samples is reproduced in the metallic sample, with the peak intensity of the pulse remaining almost constant as the pulse propagates within the material, with a progressive reduction of the pulse duration. That specific behavior thus appears to be related to the size of the α coefficient, but there is no evidence of an abrupt transition between the two regimes.

For all cases, we report in Figs. 1(b), 1(d), 1(f), and 1(h) the electronic density of the plasma created by the radiation as a function of the sample depth at a delay time of 100 fs, that is, after the end of the incoming radiation pulse. In the case of MgO and MgF_2, we report the electron density at the two wavelengths corresponding to the intensity plots. In the case of the metals, we also plot the electron density at the additional wavelength $\lambda = 100$ nm. The most evident difference is related to the presence of an exponential decay, which is evident in the case of metals and apparently absent for transparent materials, at least in the wavelength range where μ_0 is rather high. It is important to consider that the spatial distribution of the plasma density is affected by the spatial distribution of the incoming intensity.

To analyze the observed behavior in K and Fe, in those conditions where a flat density is present, we fitted an exponential function only on the final decay, as shown in Figs. 1(f) and 1(h). We found that the fitting functions are very similar to an exponential decay, which can be linked to the absorption coefficient μ_0. Indeed, in the case of potassium, the ratio of the decay coefficients $\mu_{\rm exp}$, extracted from the simulation, to μ_0, are 0.860, 0.986, and 0.816 μm^{-1}, while in the case of iron it is found that $\mu_{\rm exp}/\mu_0$ is 0.942, 0.977, and 0.982 μm^{-1}: the tight correspondence is evident. This result suggests that the spatial decay of the incoming intensity (and, thus, of the produced plasma density) behaves similarly to a normal

TABLE I. List of systems simulated using the present empirical model. The atomic number density n_{at} is the density of the first atom of the formula unit. The linear absorption coefficient μ_0, obtained from the available optical constants n and k used for the simulation, is reported together with the α parameter of Eq. (5) and the distance d_b, where the electron density of the plasma produced by the EUV pump has a sharp decrease (see text).

Sample μ_0, α	$\lambda = 20$ nm	$\lambda = 40$ nm	$\lambda = 60$ nm	$\lambda = 100$ nm	$\lambda = 110$ nm	$\lambda = 190$ nm
C $n_{at} = 0.1763$ Å^{-3}						
C $\mu_0(\lambda)$ (μm^{-1})		31.0	21.0	12.4		6.5
C $\alpha(\lambda)$ (μm^{-1})		3.51	9.07	26.7		0.09
C $d_b(\lambda)$ (μm)		0.60	0.85	1.22		1.60
MgO $n_{at} = 0.05349$ Å^{-3}						
MgO $\mu_0(\lambda)$ (μm^{-1})		76	130	63	20	
MgO $\alpha(\lambda)$ (μm^{-1})		6.07	15.55	12.58	4.38	
MgO $d_b(\lambda)$ (μm)		2.40	3.00	4.95	5.90	
MgF_2 $n_{at} = 0.03044$ Å^{-3}						
MgF_2 $\mu_0(\lambda)$ (μm^{-1})		47	154	114	135	
MgF_2 $\alpha(\lambda)$ (μm^{-1})		6.60	32.37	40.00	51.98	
MgF_2 $d_b(\lambda)$ (μm^{-1})		4.05	4.25	6.14	5.94	
K $n_{at} = 0.01322$ Å^{-3}						
K $\mu_0(\lambda)$ (μm^{-1})	0.114	0.438	0.082	0.163		0.128
K $\alpha(\lambda)$ (μm^{-1})	0.0184	0.142	0.0397	0.132		0.196
K $d_b(\lambda)$ (μm)		15.7	17.55	30.8		76.3
Fe $n_{at} = 0.08496$ Å^{-3}						
Fe $\mu_0(\lambda)$ (μm^{-1})	0.22	1.04	2.02	3.82		7.87
Fe $\alpha(\lambda)$ (μm^{-1})	0.0056	0.052	0.152	0.481		1.88
Fe $d_b(\lambda)$ (μm)		2.1	3.7	6.45		12.2
LiF $n_{at} = 0.06230$ Å^{-3}						
LiF $\mu_0(\lambda)$ (μm^{-1})	39.0	57.8				
LiF $\alpha(\lambda)$ (μm^{-1})	1.39	3.68				
LiF $d_b(\lambda)$ (μm)	1.28	2.12				

absorption process. This trend is produced by the fact that, at the end of the travel, the incoming pulse becomes shorter and shorter (see Fig. 1) and the total available energy decreases. When the pulse energy is below a critical limit, the absorption does not produce a relevant reduction of the absorption coefficient.

Considering the above results, we studied the effect of the total energy per pulse of the incoming radiation more in detail. To this purpose, we analyze the cases of MgO and Fe as a function of E_{tot} from 5 to 50 μJ, in steps of 5 μJ. The results are reported in Fig. 2, in which it is observed that the energy has a complex effect on the plasma density. In all cases, it is found that the electron density shows a rather abrupt break when becoming lower than a practically fixed value n^b_{pl}. This behavior is sketched in Figs. 2(a) and 2(c) as a horizontal dashed line at $n^b_{pl} = 0.0045$ Å^{-3} in MgO and at $n^b_{pl} = 0.0053$ Å^{-3} in Fe. Considering the huge difference in the absorption coefficient μ_0 in the two materials (see Table I), we can state that the effect does not depend on μ_0, since the n^b_{pl} values retrieved are rather similar. One can thus guess that this behavior is due to a mixture of contributions: while iron has a much smaller absorption coefficient than magnesium oxide, it has a larger atomic density.

Another complex effect is related to the trend of the density as a function of space. In the case of Fe, in which μ_0 is low, $n_{pl}(x)$ is practically constant up to a break distance d_b,

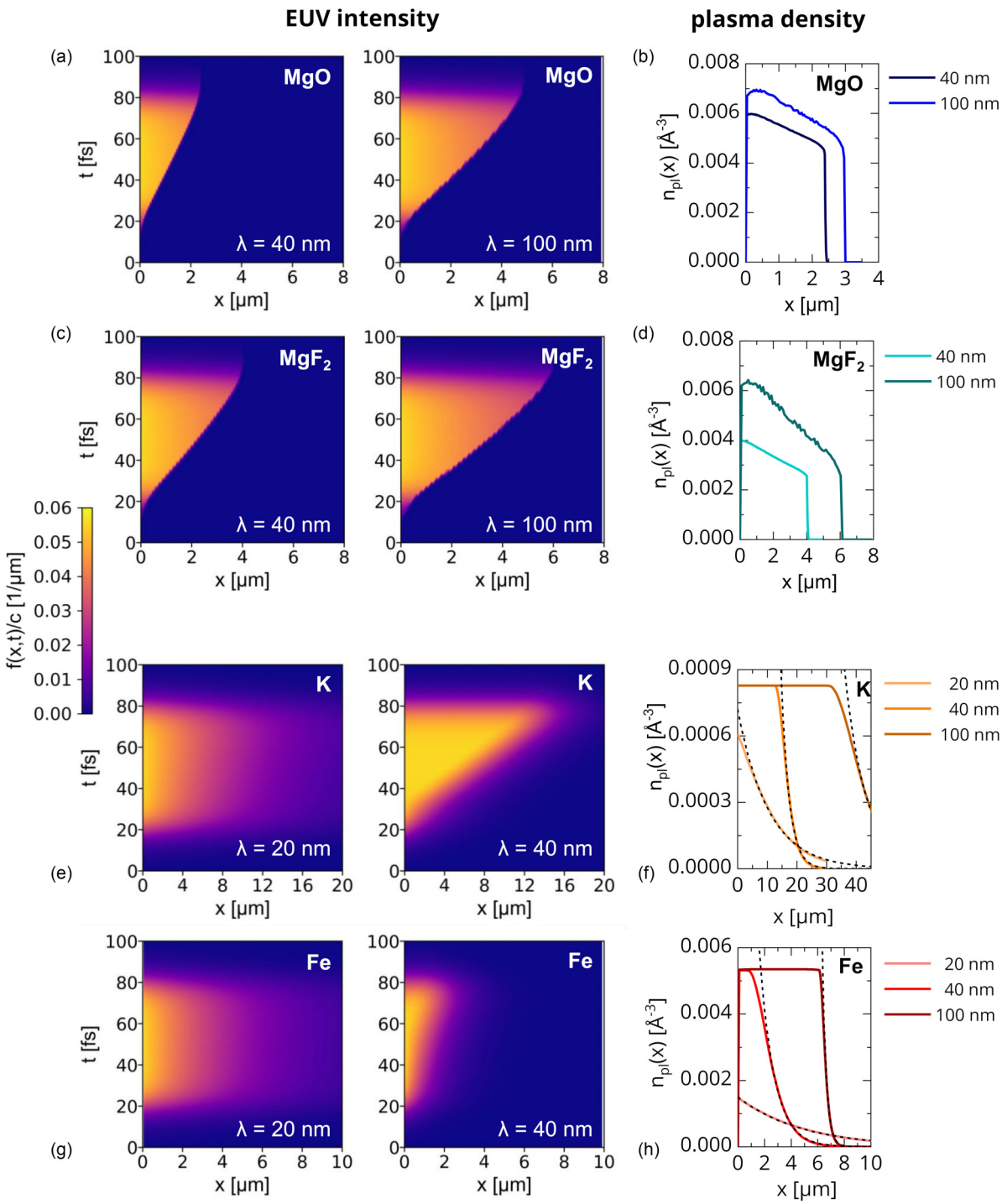

FIG. 1. Space-time evolution of the radiation intensity in (a) MgO, (c) MgF_2, (e) K,and (g) Fe at two different wavelengths, as indicated by the labels. [(b), (d), (f), and (h)] Spatial distribution of the plasma electron density 100 fs *after* the mean time of the EUV pulse, at the same wavelengths as the intensity distributions. An additional wavelength ($\lambda = 100$ nm) is also reported in the case of K and Fe, where an exponential decay is present. The dashed black lines are exponential fits to the electron density in the region of nearly exponential decay, with decay constant $\mu_{\rm exp}$.

above which a clear decrease is seen, followed by an exponential decay. In contrast, in the case of MgO, in which μ_0 is high, it is seen that, at growing depth, the electron density tends to decrease, with a quite evident energy dependence. At low energy, the fractional decrease of $n_{\rm pl}(x)$ is rather small, because the value $n^b_{\rm pl}$ (blue dashed line of Fig. 2) does not depend on the energy of the incoming pulse. However, the value of $n_{\rm pl}(x)$ in the region close to the external sample surface increases on increasing $E_{\rm tot}$ and, as a consequence, the fractional density variation becomes larger. To quantify this effect, in Fig. 2(b) we plot the $E_{\rm tot}$ dependence of the difference $n_{\rm pl}(x_M) - n^b_{\rm pl}$, x_M being the position of the density

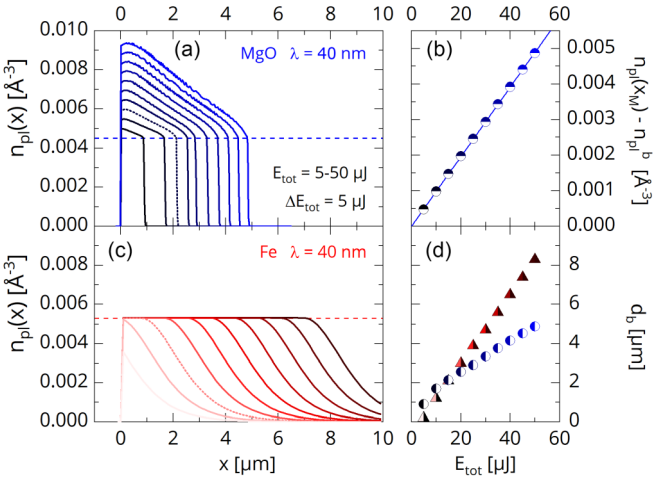

FIG. 2. (a) Space evolution of the plasma electron density $n_{\rm pl}(x)$ in MgO determined at $t = 100$ fs, at $\lambda = 20$ nm, at varying the total pulse energy, with $E_{\rm tot}$ from 5 to 50 μJ in steps of 5 μJ, reported in blue shades, with lighter colors for higher energies. The horizontal blue dashed line indicates the electron density $n_{\rm pl}^b$ where the energy-independent break of $n_{\rm pl}(x)$ is observed (see text). The dotted line is used for the case $E_{\rm tot} = 15$ μJ, further explored in Fig. 4. (b) Excess of density $n_{\rm pl}(x_M) - n_{\rm pl}^b$ in MgO with respect to the reference value $n_{\rm pl}^b$, blue dots. The blue line is a linear fit through the origin. x_M indicates the position where the density has its maximum. (c) Same as in (a) for Fe at $\lambda = 40$ nm. (d) Energy dependence of the density break distance d_b (see text for details) in MgO (blue dots) and Fe (red triangles). The color palette is according to (a) and (c).

maximum. As is evident from the plot, there is a linear dependence on the pulse energy. Therefore, one can guess that there is a *proper* absorbed energy per unit length which produces an *equilibrium* plasma density, while the excess of absorbed energy produces an excess density, which decreases with the pulse energy penetrating the sample.

As further information, we plot in Fig. 2(d) the break distance d_b, defined as the position of the maximum of $-dn_{\rm pl}(x)/dx$ as a function of $E_{\rm tot}$. It is found, as expected, that d_b is an increasing function of $E_{\rm tot}$ and it is generally higher in Fe, low-absorbing material, than in MgO, high-absorbing material. However, the global trend cannot be interpreted in a simple way. Indeed, at low energy d_b tends to be greater in MgO than in Fe.

In metals, particularly in Fe, the pulse is almost uniformly absorbed over time, so that the residual pulse duration has a mild dependence on the depth inside the sample. Therefore, it is evident that the sharp plasma density decrease observed in transparent materials is linked to the region where the residual pulse duration becomes short. This behavior is present when μ_0 is large enough. Indeed, all the process is based on the fact that, as the plasma is created, the absorption coefficient immediately decreases (a condition specific to the EUV range), because the electron plasma has normally a relatively small plasma frequency, which also behaves as absorption cutoff. Therefore, the radiation pulse shortening, typical of the high-absorption materials, occurs only if enough electrons are excited per unit length. Assuming that a fraction α^* of the electrons is necessary to make the material transparent,

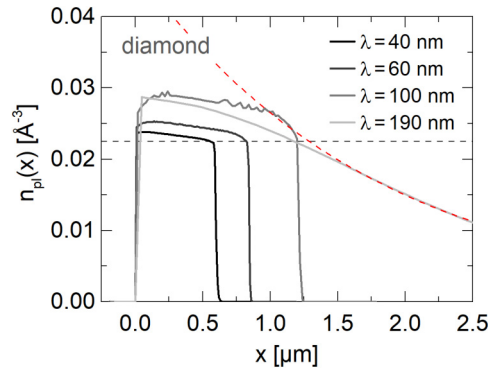

FIG. 3. Space evolution of the plasma electron density in diamond at four different wavelengths and $E_{\rm tot} = 15$ μJ. The wavelengths are 40, 60, 100, and 190 nm (gray solid lines, from dark to bright). The horizontal dashed line marks the break in the electron density $n_{\rm pl}^b$, which is wavelength independent, as observed for other materials. The red dashed line is an exponential fit to the data at $\lambda = 190$ nm and at $x > 1.5$ μm.

the whole process becomes effective if $N_0\,\mu_0/S$ is larger than $\alpha^* n_{\rm at}$, S being the pulse diameter. If the condition is not fulfilled, the absorption proceeds without creating a significant plasma density, the behavior of the material remains uniform, and the duration of the pulse is not modified. When the absorption is high, the process continues with the creation of an almost uniform plasma until the residual duration of the radiation pulse becomes very short, and the creation process stops suddenly.

Finally, we applied the model to the case of diamond. The major difference of diamond with respect to the other materials is its significantly larger atomic density. The simulation results are reported in Fig. 3, where it is seen that the plasma electron density behaves in a similar way as the other transparent materials apart from the fact that, at long wavelength, because of the reduction of μ_0 on approaching the visible region where the sample is transparent, no plateau is present and the density exponentially decays. Again, the exponential decay has a decay constant similar to μ_0, $\mu_{\rm exp} \sim 0.587$ μm^{-1} as compared to $\mu_0 = 0.6$ μm^{-1} (tabulated value).

A. Effect of core hole lifetime on the plasma formation

The model described above neglects the effect of the lifetime of the core holes produced by the absorption process. Core hole annihilation can occur (1) by radiative decay, involving two electron states and one photon state, and (2) through Auger decay, involving four electron states and no photon state. Usually, the radiative decay is a relatively slow process, while the core hole annihilation via Auger decay is faster. The complexity of the Auger process makes the evaluation of a core hole lifetime a quite difficult task. Calculations of Auger rates in simple molecules are possible [23–25], and it is found that light molecular systems, like LiF or water, have a state-dependent decay lifetime, varying from tens to hundreds of femtoseconds.

The experimental determination of the core hole lifetime, which is fairly difficult already in stationary conditions, becomes even harder in a time-resolved experiment. Therefore,

we modified the model to have a preliminary evaluation of the effect of the localized state lifetime on the plasma evolution. The evolution of the core hole population is complex, but it can be described by an inverse lifetime $\Gamma_r = 1/\tau_r$, which is due to different processes like radiative and Auger recombination. If different processes give rise to the core hole decay, they globally result in a single inverse lifetime $\Gamma_r = \sum_i 1/\tau_i$, so that one has

$$dZ = \Gamma_r[Z_0 - Z(t)]\,dt. \tag{7}$$

We recall that, as it is well known, starting from an initial state in which the excitation has produced a core state average population $Z_i < Z_0$, in the absence of further excitation, the time evolution of the population is very simple:

$$Z(t) = Z_0 + (Z_i - Z_0)\exp[-\Gamma_r t]. \tag{8}$$

This result is valid if $Z_0 - Z_i \ll Z_0$, because an excess of excitation produces a hot plasma, with a progressive loss of the system structure and a reduction of the hole recombination rate.

In any case, assuming a fixed inverse lifetime, if the incident radiation is active, the time evolution of $Z(x,t)$ is a variant of the previous equation:

$$dZ = \{-\alpha f(x,t) + \Gamma_r[Z_0 - Z(x,t)]\}dt. \tag{9}$$

This time evolution of the core-state population produces a modification of Eq. (4), and the evolution of the linear absorption coefficient becomes

$$d\mu = \frac{\nu}{Z_0}\mu_0\{-\alpha f(x,t) + \Gamma_r[Z_0 - Z(x,t)]\}dt. \tag{10}$$

Looking at Eq. (10) it is evident that there can be a complex effect of the core hole lifetime. Indeed, this process tends to *reduce* the decrease of the core-state population and, hence, of $\mu(x,t)$, at a given spatial point. However, the lower decrease of the absorption coefficient produces, at the same time, an increase of N_t [see Eq. (3)] with a corresponding decrease of $Z(x,t)$. Therefore, the finite lifetime of the core hole has the combined effect of decreasing and increasing the core state population as a function of time.

The effect of Γ_r has been estimated in the case of MgO and Fe, as typical examples of systems having high and low absorption, respectively. The value of the lifetime τ_r has been varied in the range 5–50 fs, that is, Γ_r is varied from 0 to 0.2 fs^{-1}. The resulting electron plasma density, as determined at $t = 100$ fs using $E_{\rm tot} = 15$ μJ, is reported in Fig. 4. Of course, on increasing the delay time other processes should be taken into account, but the contribution of the nuclear motion is not considered relevant in this time range.

The results in Fig. 4 show a very different behavior in the two systems MgO and Fe. In the high-absorption compound MgO, it is found that the core hole lifetime has a similar effect in all cases with an abrupt (spatially limited to <100 nm) increase of the density up to an almost constant level extending in a wide distance range, followed by a rather sharp peak at the end of the plasma region. The steep initial jump remains constant, no matter what the value of Γ_r is; the flat density decreases on increasing Γ_r, down to rather low values; and also the final peak decreases, but with a lower rate. The initial flat region in the density plot as a function of x is created

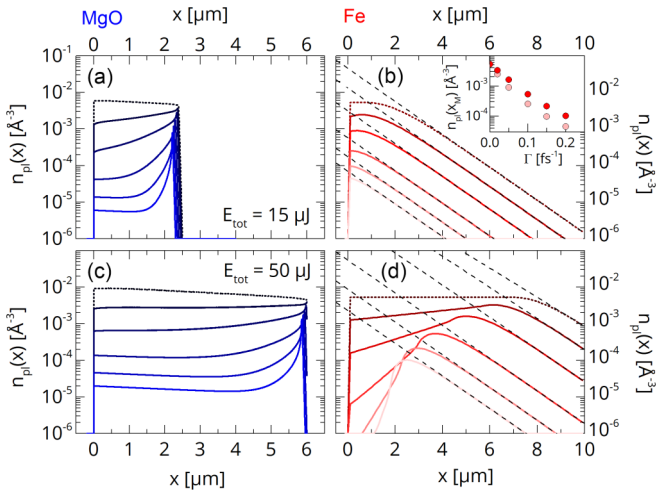

FIG. 4. Space evolution of the plasma electron density in (a and c) MgO and (b and d) Fe, determined with $E_{\rm tot} = 15$ μJ [(a) and (b)] and $E_{\rm tot} = 50$ μJ [(c) and (d)], at $\lambda = 40$ nm at $t = 100$ fs. The curves show data at varying Γ_r, from top to bottom (and from dark to light color): 0 (dotted lines), 0.02, 0.05, 0.10, 0.15, and 0.2 fs^{-1}. The inset of (b) reports the $n_{\rm pl}(x_M)$ at the position x_M where the density has its maximum for $E_{\rm tot} = 15$ μJ (pink dots) and $E_{\rm tot} = 50$ μJ (red dots).

by the initial part of the incoming EUV light pulse so that, on reducing the core hole lifetime, it is subject to a higher decrease because of the core hole–electron recombination. On the other hand, the peak is created at a time closer to the observation time of 100 fs, so that the recombination has a smaller effect.

In the case of iron, a low-absorption metal (MgO, $\mu_0 = 76$ μm^{-1}, Fe, $\mu_0 = 1$ μm^{-1}), the plasma density is distributed in a different way. Indeed, the initial increase is mild, up to a maximum followed by a slow decrease. As a consequence, the data show a smooth maximum increasing on increasing the lifetime (i.e., decreasing Γ_r). The maximum practically disappears when $\Gamma_r = 0$ (dotted curves), as is also the case of MgO.

An intriguing shared feature of both MgO and Fe is the final decline rate, which is well described by an exponential trend of the form $\propto \exp[-\mu_0 x]$, independently of $E_{\rm tot}$ and of the core hole lifetime, steep in the case of MgO and slow in Fe. Across the explored range of $E_{\rm tot}$ and Γ_r, no indication of deviation from the trend is present, although the specific range in which the trend appears varies depending on both parameters. For instance, the sharp decrease observed in MgO maintains its rate but its spatial extent is influenced by $E_{\rm tot}$, while only a small dependence on Γ_r is observed, as already evident in Fig. 4.

Finally, the peak electron density is considered [inset of Fig. 4(b)], produced in the different cases as a function of Γ_r at fixed energy $E_{\rm tot}$. It is found that in iron the peak electron density increases by a large factor [$F = x_M(\Gamma_r = 0.02\ \text{fs}^{-1})/x_M(\Gamma_r = 0.2\ \text{fs}^{-1})$] at decreasing Γ_r from 0.2 fs^{-1} (lifetime 5 fs) down to 0.02 fs^{-1} (lifetime 50 fs). F decreases from 55 to 32 on increasing $E_{\rm tot}$ from 15 to 50 μJ. In the case of MgO (data not shown), there is a similar trend but the effect is much smaller, with F ranging from 4.6 to 3.0 on increasing $E_{\rm tot}$ from 15 to 50 μJ.

It is also important to consider that, in a real case, the strong excitation of the material after energy absorption does not change the absorption coefficient only. Indeed, considering that the electron states with low binding energy are largely modified by the radiation, also the core hole lifetime is expected to change during the excitation process. This specific process needs a precise description of this (dynamic) plasma state to be accounted for.

B. Qualitative and quantitative comparison to real experiments

Our model describes the effects of a FEL pump in the x-ray/EUV range on the absorption coefficient of the sample, suggesting that the produced changes can be probed with photons in the optical range (x-ray/EUV pump optical probe), at least for materials that are insulating in the ground state. As mentioned above, several experiments in the literature show x-ray/EUV FEL pulses inducing mechanisms similar to those discussed here. The FEL pumping effects are there investigated in transmission [15–18,26], and in two color FEL pump-probe diffraction [27,28] and photoemission [29] schemes. In Ref. [28], Allaria *et al.* reported a significant attenuation of the probe contribution in the diffraction pattern of a Ti dispersive grating induced by a 38-nm pump at high fluence (in the order of 1 J/cm^2, which is compatible with the conditions explored here). This effect was associated with the FEL-induced ionization of Ti atoms, resulting in a reduction of the absorption coefficient near the pump wavelength. Similar effects of photoinduced transparency caused by high-fluence ($\sim 10^4$ J/cm^2) FEL pulses were also reported in Ref. [27], where an attenuation of the probe diffraction peak was observed in diamond on a timescale of $\sim$10 fs, and in Ref. [26]. In the latter study, a direct measurement of the absorption coefficient of Al was conducted using a transmission scheme with subpicosecond soft x-ray pulses at variable fluences in the range of 10^{-1}–10^2 J/cm^2. An increase in Al transmission was observed at fluences above 10 J/cm^2 due to the inner L-shell photoionization rate surpassing the e-h recombination rate. Finally, the attosecond x-ray pump-probe measurement in Ref. [29] directly probes by electron photoemission spectroscopy the increase in the binding energy of electrons in the carbon K-shell, upon photoionization of para-aminophenol. Of course, the design of such experiments was not explicitly aimed at proving the validity of our model, but their interpretation is qualitatively in line with the description proposed here, thus corroborating our approach.

As a more suitable experimental example to directly test the present model, we refer to the investigation performed on a crystalline sample of lithium fluoride [10]. In this experiment, a beam of 15 μJ per pulse with $\lambda = 37.14$ nm, a spot diameter of $\sim$30 μm, and a duration of $\sim$80 fs is produced at the elastic inelastic scattering (EIS)-TIMEX beam line [13] (FERMI FEL [3], Trieste, Italy). This beam was used to produce a plasma excitation, with results useful to gain experimental insights into the EUV plasma creation process. The pump and probe experiment provided the optical transmission as a function of time. From the optical transmission, it is possible to derive some information on the electron plasma, which is nearly transparent to the EUV pump but absorbs in the visible and near-UV region [10]. This specific experiment, exploiting the initial transparency of the sample in the optical region, was originally devoted to the investigation of the evolution of the plasma in the 1–2-ps time range after the arrival of the EUV pulse.

Here, we confine our study to the time interval just after the arrival of the EUV pump. A supercontinuum pulse in the range 450–730 nm is employed to measure the plasma transmission. From the transmission experiment, in ideal conditions, one can determine the product between the linear absorption coefficient and the plasma thickness $\mu_0(\lambda)d_b$. While in principle the reflectivity of the plasma might limit the measurement accuracy, an estimate of the plasma optical coefficients suggests that this effect plays only a minor role [10].

Using the model described above, the simulation of the LiF sample was performed considering an EUV pulse with the characteristics of the experiment and, for comparison purposes, also a pulse at $\lambda = 20$ nm. The LiF simulation data are reported in Table I; the data related to the experiment at $\lambda = 37.14$ nm are found in the column labeled 40 nm. The plasma density resulting from the simulations is presented in Fig. 5(a), in which a behavior similar to that of MgO and MgF_2 is observed, with $n_{\rm pl}(x)$ showing an extended plateau and a break at a density independent of the exciting wavelength.

The simulation was carried out without any reference to experiments, apart from the use of tabulated optical constants of the material considered in the initial state. It is found that the obtained value of $d_b = 2.12$ μm (see Table I) compares well with the experimental estimate [10]. Furthermore, the magnitude of the electron density in the plasma is in reasonable agreement with the average density deduced from the complex, long-time evolution observed in the experiment.

Considering that in the real experiment the intensity of the pump is not spatially uniform, because the pump beam has a Gaussian intensity profile, the effect of the beam energy $E_{\rm tot}$ was also simulated using the model. The results of the simulation, in Fig. 5(b), expectedly show a behavior similar to that of MgO (see Fig. 2), with a smooth increase of both density and thickness on increasing $E_{\rm tot}$, as well as a break of the electron density at a fixed value. In Fig. 5(b), a limited increase of the average density is observed as a function of the energy [see also Fig. 5(d)].

The effect of the core hole lifetime is also evaluated in the same conditions of the experiment, safely assuming a lifetime of 50 fs. Immediately after the EUV excitation, the actual core hole lifetime is probably even longer, because of the effect of the excited, almost free, electron states present in the plasma. From the results, shown in Fig. 5(e), it is evident that the plasma thickness is independent of Γ_r, but the electron density distribution is changed. Therefore, one can expect to derive very useful information by measuring the transmission of the plasma in the wavelength interval where the original LiF crystal is almost ideally transparent. In particular, we see that the plasma electron density is less uniform in condition where the core hole lifetime is shorter. When the plasma density is not uniform, one might expect a relevant contribution associated with electron diffusion. However, assuming that quantum mechanics plays a minor role, in the present timescale where $t \approx 100$ fs, considering an average plasma electron energy of $\sim$100 eV, the average electron velocity results to be less than 2 μm/ps, with randomly distributed

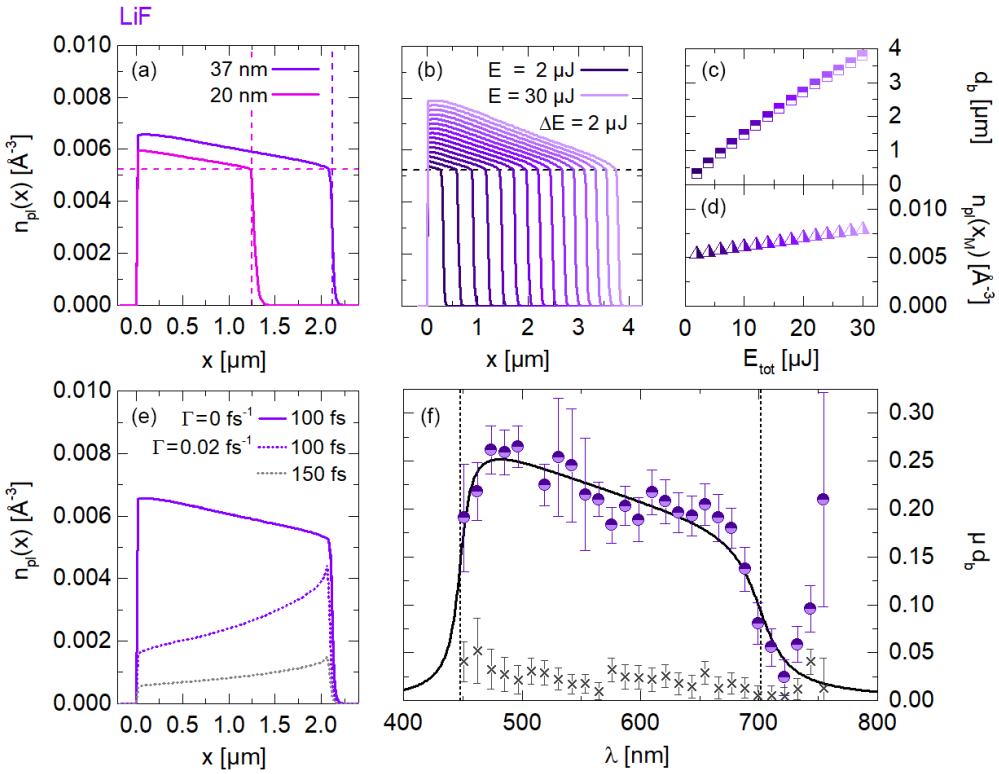

FIG. 5. (a) Space evolution of the plasma electron density in LiF determined with $E_{\rm tot} = 15\,\mu$J at $t = 100$ fs, at 20 nm (pink) and 37.14 nm (violet line). The horizontal dashed line indicates $n_{\rm pl}^b$. The vertical dashed lines indicate the thickness of the plasma (d_b) at 20 nm (pink) and 37 nm (violet). (b) Energy dependence of the plasma density in LiF, at $t = 100$ fs and $\lambda = 37.14$ nm. The energy is increased from $E_{\rm tot} = 2\,\mu$J (dark line) up to $E_{\rm tot} = 30\,\mu$J (light line) in steps of $2\,\mu$J, and the corresponding $n_{\rm pl}(x)$ are plotted. As in (a), $n_{\rm pl}^b$ is indicated by the horizontal dashed line. The energy dependence of d_b [(c), squares] and of $n_{\rm pl}(x_M)$ [(d), triangles] are shown in the same color scale of (b). (e) Typical effect of the core hole lifetime at $\lambda = 37.14$ nm and $E_{\rm tot} = 15\,\mu$J. The $\Gamma_r = 0$ result at $t = 100$ fs (dark solid line) is compared to the results with $\Gamma_r = 0.02$ fs^{-1} (dotted line, dark) and, with the same parameters, also at $t = 150$ fs (dotted line, light). (f) Product $\mu(\lambda)d_b$ deduced from the experiment [10]. The data at small negative time, which measure the efficiency of the instrument, are reported as gray crosses, while the data taken at a small delay (100–200 fs) after the EUV pump are shown as violet dots. The black solid line shows a data fit using the simple model described in the text. The vertical dashed lines indicate the minimum ($\lambda_{\rm min}$) and maximum ($\lambda_{\rm max}$) wavelengths as obtained from the fit (see text).

direction, which is a rather small value in comparison to the density variations shown in Fig. 5(e). Therefore, we consider the present description adequate to the purpose of studying the plasma just after its creation.

To perform an analysis of the experimental data, we start from the calculation of Ref. [21], assuming that the absorption is also proportional to the number of electrons in the absorption volume. In addition, from Fig. 5(e), we can reasonably consider the product $n_{\rm pl}\,\omega_p$ as roughly constant in the range where the density is not very small, producing a detectable absorption of the probe radiation. Using these approximations and describing the ideal plasma resonance with a Lorentzian function, it is possible to describe $\mu(\omega)d_b$ in a closed form, considering a uniform distribution of plasma frequencies between $\omega_m - \Delta$ and $\omega_m + \Delta$. Such lineshape is appropriate for a simple comparison to the experimental data. We found

$$\mu(\omega)d_b = \frac{\mu(\omega_m)\,d_b\,\omega}{2\pi\,\Delta}\left[\arctan\left(\frac{\omega_m - \omega + \Delta}{\Gamma_p}\right) - \arctan\left(\frac{\omega_m - \omega - \Delta}{\Gamma_p}\right)\right], \tag{11}$$

where $\omega_m = \sqrt{12/r_s^3}$ is the plasma frequency in Rydberg units at the average density and Γ_p is the damping function, assumed to be constant. The factor ω is due to the proportionality to the photon energy of the photoelectric effect transition rate. This equation can be used to describe the experimental data shown in Fig. 5(f).

A more complex and accurate approximation could be performed using an estimate of the plasma dielectric function, but such an approach is rather complex also because temperature effects need to be considered [30].

The radiation absorption in the EUV range and beyond produces a relatively low plasma density because the absolute maximum of $n_{\rm pl}(x,t)$ is $Z_0 n_{\rm at}$. By assuming only one excited electron per Li atom, the expected maximum electron density corresponds to $r_s \simeq 2.96$ and the maximum plasma frequency is $\hbar\omega_p \simeq 9.27$ eV, still a rather low value which produces a negligible absorption of radiation at energy beyond 20–30 eV. On the other hand, the so-produced plasma is absorbing at lower energy, an effect quite evident if the original material is transparent in the same range, as in the case of LiF and the other insulating materials considered here.

To perform a tentative comparison to the experimental results of the sample transmission in the visible region, we used the available data from Ref. [10], deriving the wavelength dependence of the plasma transmission in a small time window after the EUV pulse arrival. By averaging the data in the delay range $\sim$ 100–200 fs, we obtain the results shown in Fig. 5(f), in which we report the product $\mu(\lambda)d_b = -\ln[T(\lambda)]$, $T(\lambda)$ being the observed sample transmission for the radiation at a given wavelength λ. In Fig. 5(f), we also report the raw transmission measured at negative delay with $t < -100$ fs. It is evident that the sample, without EUV excitation, has almost no absorption in this wavelength range, and the data clearly show the high transmission of LiF. Accordingly, data at negative delay were used as a transfer function of the instrument for a minor correction. Looking at Fig. 5(f), we find a mild wavelength dependence of $\mu(\lambda)d_b$. Therefore, for a preliminary estimate of μ_0, we consider the average of $\mu(\lambda)d_b$ in the range 480 nm $< \lambda <$ 660 nm. Assuming a thickness of the plasma $d_b = 2.12\,\mu$m, as determined from the simulation (see Table I), we find $\langle\mu\rangle = 0.103 \pm 0.003\,\mu\text{m}^{-1}$.

Considering the shape of the absorption versus the wavelength presented in Fig. 5(f), we believe that there is evidence of a nonuniform electron density. Indeed, if the plasma had a well-defined density, one would expect a relatively sharp absorption peak at the energy $\hbar\omega_p(r_s)$, while the observed wavelength range corresponds to about $6 < r_s < 8$ at zero temperature. According to Eq. (11), the observation can be related to the fact that the intensity of the EUV pulse is not spatially uniform and the decrease of μd_b on increasing λ can be attributed to the wavelength [energy, according to Eq.(11)] dependence of μ. Actually, there is no experimental information about the intensity variation in the volume sampled by the probe beam. Therefore, considering that the probed volume is smaller than the volume where the pump acts, we assumed that the plasma density has a smooth variation in a given region, so that the plasma wavelength can be assumed to vary between $\lambda_{\min} = 2\pi c/(\omega_m + \Delta)$ and $\lambda_{\max} = 2\pi c/(\omega_m - \Delta)$ with a constant weight apart from a factor proportional to the photon energy. In this way, we assume that the simple analytic form of Eq. (11) is adequate to describe the present experimental data of $\mu(\omega)d_b$. The fit of Eq. (11) to experimental data is shown in Fig. 5(f), and the good agreement with the experimental data is evident.

We found that the plasma absorption is relevant in the range between $\lambda_{\min} = 448 \pm 4$ nm and $\lambda_{\max} = 702 \pm 10$ nm, corresponding to $r_s = 6.62 \pm 0.04$ and $r_s = 8.93 \pm 0.08$. The average density observed in the simulation of Fig. 5(a) provides $r_s = 6.45$, a value close to the maximum density of the fit to the data. However, the effect of the core hole lifetime plays a major role in determining the variation of the electron density, so that one can guess that the estimates from the fit are providing an interesting clue about the formation and initial stability of the plasma. Considering that the experimental data were not specifically collected for this sort of analysis, we believe that the experiment provides good support to the description of the plasma formation using a high-energy pump.

IV. CONCLUSION

We have presented an empirical approach to describe the absorption of an intense and short EUV or soft x-ray pulse in crystalline samples, having in mind the description of the initial phase, when the electron-ion interaction plays a negligible role. A first-principle detailed description of the excitation process is extremely complex. This holds for all materials, from metals to insulators, and including semiconductors [31], the complexity arising from the variety of processes that can be triggered by EUV light [32]. Indeed, while it is possible, at some level of accuracy, to consider the effect of empty core states, the behavior of the electron excited states is much more demanding to model [32–34]. These two basic processes are going to produce opposite effects, as the transition rate is expected to be reduced by the excitation of core states, while it can be raised by the increased number of final states available in the excited electron gas.

We tried to take into account experimental absorption data obtained on normal state materials, exploiting an empirical description of the change in the absorption coefficient in different excitation conditions. Using different choices for the parameters of the model, the complex interplay of the different contributions is shown. The model can be useful to perform an analysis of the experimental data to identify the important effects to be taken into account. The application in the case of different materials allows understanding the role of the specific properties of the excited materials.

An experimental description of the change of the transmission of crystalline LiF is shown in the visible region after 100 fs from the arrival of a 70-fs pulse of EUV radiation at 31 eV. The model was found to compare well with the experiment, providing information otherwise unaccessible on the sample behavior.

The authors declare no conflicts of interest.

ACKNOWLEDGMENTS

E.S. acknowledges funding from Project ECS 0000024 Rome Technopole, CUP B83C22002820006, NRP Mission 4 Component 2 Investment 1.5, Funded by the European Union NextGenerationEU.

[1] P. Emma *et al.*, First lasing and operation of an Ångström-wavelength free-electron laser, Nat. Photon. **4**, 641 (2010).

[2] T. Ishikawa *et al.*, A compact X-ray free-electron laser emitting in the sub-Ångström region, Nat. Photon. **6**, 540 (2012).

[3] E. Allaria *et al.*, Highly coherent and stable pulses from the FERMI seeded free-electron laser in the extreme ultraviolet, Nat. Photonics **6**, 699 (2012).

[4] C. Bostedt, S. Boutet, D. M. Fritz, Z. Huang, H. J. Lee, H. T. Lemke, A. Robert, W. F. Schlotter, J. J Turner, and G. J. Williams, Linac coherent light source:

The first five years, Rev. Mod. Phys. **88**, 015007 (2016).

[5] N. Huang, H. Deng, B. Liu, D. Wang, and Z. Zhao, Features and futures of X-ray free-electron lasers, Innovation **2**, 100097 (2021).

[6] C. Fasolato, E. Stellino, E. Principi, R. Mincigrucci, J. S. Pelli-Cresi, L. Foglia, P. Postorino, F. Sacchetti, and C. Petrillo, Superradiant Thomson scattering from graphite in the extreme ultraviolet, Proc. Natl. Acad. Sci. USA **121**, e2221293121 (2024).

[7] Z. Chen *et al.*, Observation of a highly conductive warm dense state of water with ultrafast pump–probe free-electron-laser measurements, Matter Radiat. Extremes **6**, 054401 (2021).

[8] L. Chopineau, A. Leblanc, G. Blaclard, A. Denoeud, M. Thévenet, J. L. Vay, G. Bonnaud, P. H. Martin, H. Vincenti, and F. Quéré, Identification of coupling mechanisms between ultraintense laser light and dense plasmas, Phys. Rev. X **9**, 011050 (2019).

[9] G. De Ninno, B. Mahieu, E. Allaria, L. Giannessi, and S. Spampinati, Chirped seeded free-electron lasers: self-standing light sources for two-color pump-probe experiments, Phys. Rev. Lett. **110**, 064801 (2013).

[10] C. Fasolato *et al.*, Ultrafast plasmon dynamics in crystalline LiF triggered by intense extreme UV pulses, Phys. Rev. Lett. **124**, 184801 (2020).

[11] G. Rohde, A. Stange, A. Müller, M. Behrendt, L. P. Oloff, K. Hanff, T. J. Albert, P. Hein, K. Rossnagel, and M. Bauer, Ultrafast formation of a Fermi-Dirac distributed electron gas, Phys. Rev. Lett. **121**, 256401 (2018).

[12] H. Kitamura, Third-order nonlinear effects on femtosecond x-ray-absorption near-edge spectra, Phys. Rev. A **102**, 023120 (2020).

[13] C. Masciovecchio *et al.*, EIS: the scattering beamline at FERMI, J. Synchrotron Radiat. **22**, 553 (2015).

[14] E. D. Palik, *Handbook of Optical Constants of Solids*, (Academic, New York, 1998), Vol. 3.

[15] H. Yoneda *et al.*, Ultra-fast switching of light by absorption saturation in vacuum ultra-violet region, Opt. Express **17**, 23443 (2009).

[16] Y. Inubushi *et al.*, Note: Measurement of saturable absorption by intense vacuum ultraviolet free electron laser using fluorescent material, Rev. Sci. Instrum. **81**, 036101 (2010).

[17] A. Di Cicco, K. Hatada, E. Giangrisostomi, R. Gunnella, F. Bencivenga, E. Principi, C. Masciovecchio, and A. Filipponi, Interplay of electron heating and saturable absorption in ultrafast extreme ultraviolet transmission of condensed matter, Phys. Rev. B **90**, 220303(R) (2014).

[18] H. Yoneda, Y. Inubushi, M. Yabashi, T. Katayama, T. Ishikawa, H. Ohashi, H. Yumoto, K. Yamauchi, H. Mimura, and H. Kitamura, Saturable absorption of intense hard X-rays in iron, Nat. Commun. **5**, 5080 (2014).

[19] E. Runge and E. Gross, Density-functional theory for time-dependent systems, Phys. Rev. Lett. **52**, 997 (1984).

[20] M. A. L. Marques, N. T. Maitra, F. M. S. Nogueira, E. K. U. Gross, and A. Rubio, *Fundamentals of Time-Dependent Density Functional Theory* (Springer, New York, 2012), Vol. 837.

[21] M. Finazzi and F. K. U. Ciccacci, Plasmon-photon interaction in metal nanoparticles: Second-quantization perturbative approach, Phys. Rev. B **86**, 035428 (2012).

[22] J. Duris *et al.*, Tunable isolated attosecond x-ray pulses with gigawatt peak power from a free-electron laser, Nat. Photon. **14**, 30 (2020).

[23] K. Zähringer, H. -D. Meyer, and L. S. Cederbaum, Angularly resolved Auger rates of LiF and HF, Phys. Rev. A **46**, 5643 (1992).

[24] E. Pahl, L. S. Cederbaum, H. D. Meyer, and F. Tarantelli, Controlled interplay between decay and fragmentation in resonant Auger processes, Phys. Rev. Lett. **80**, 1865 (1998).

[25] F. Matz and T. C. Jagau, Molecular Auger decay rates from complex-variable coupled-cluster theory, J. Chem. Phys. **156**, 114117 (2022).

[26] B. Nagler *et al.*, Turning solid aluminium transparent by intense soft x-ray photoionization, Nat. Phys. **5**, 693 (2009).

[27] I. Inoue, Y. Inubushi, T. Sato, K. Tono, T. Katayama, T. Kameshima, K. Ogawa, T. Togashi, S. Owada, Y. Amemiya, T. Tanaka, T. Hara, and M. Yabashi, Observation of femtosecond X-ray interactions with matter using an X-ray–X-ray pump–probe scheme, Proc. Natl. Acad. Sci. USA **113**, 1492 (2016).

[28] E. Allaria *et al.*, Two-colour pump–probe experiments with a twin-pulse-seed extreme ultraviolet free-electron laser, Nat. Commun. **4**, 2476 (2013).

[29] Z. Guo *et al.*, Experimental demonstration of attosecond pump–probe spectroscopy with an X-ray free-electron laser, Nat. Photon. **18**, 691 (2024).

[30] C. Fortmann, Single-particle spectral function for the classical one-component plasma, Phys. Rev. E **79**, 016404 (2009).

[31] F. Rossi and T. Kuhn, Theory of ultrafast phenomena in photoexcited semiconductors, Rev. Mod. Phys. **74**, 895 (2002).

[32] S. M. Vinko, G. Gregori, M. P. Desjarlais, B. Nagler, T. J. Whitcher, R. W. Lee, P. Audebert, and J. S. Wark, Free–free opacity in warm dense aluminum, High Energy Density Phys. **5**, 124 (2009).

[33] H. Kitamura, Rapid energy-level shifts in metals under intense inner-shell photoexcitation, High Energy Density Phys. **8**, 66 (2012).

[34] P. D. Ndione, S. T. Weber, D. O. Gericke, and B. Rethfeld, Nonequilibrium band occupation and optical response of gold after ultrafast XUV excitation, Sci. Rep. **12**, 4693 (2022).